

# Optimal generation of delay-controlled few-cycle pulses for high harmonic generation in solids

Cite as: Appl. Phys. Lett. **120**, 121105 (2022); <https://doi.org/10.1063/5.0085472>

Submitted: 17 January 2022 • Accepted: 12 March 2022 • Published Online: 24 March 2022

Yabei Su,  Shaobo Fang, Shuai Wang, et al.



View Online



Export Citation




CrossMark

## ARTICLES YOU MAY BE INTERESTED IN


[Quasi 2D perovskite single-mode vertical-cavity lasers through large-area film transfer](#)  
Applied Physics Letters **120**, 121104 (2022); <https://doi.org/10.1063/5.0085882>

[Structural and thermal analysis of polycrystalline diamond thin film grown on GaN-on-SiC with an interlayer of 20nm PECVD-SiN](#)  
Applied Physics Letters **120**, 121603 (2022); <https://doi.org/10.1063/5.0083841>

[Stoichiometry-dependent surface electronic structure of SrTiO<sub>3</sub> films grown by hybrid molecular beam epitaxy](#)  
Applied Physics Letters **120**, 121604 (2022); <https://doi.org/10.1063/5.0082636>



**HIDEN**  
ANALYTICAL



40  
YEARS  
1982 - 2022


## Instruments for Advanced Science

- Knowledge,
- Experience,
- Expertise

Click to view our product catalogue


Contact Hiden Analytical for further details:  
[www.HidenAnalytical.com](http://www.HidenAnalytical.com)  
[info@hideninc.com](mailto:info@hideninc.com)

Gas Analysis




- ▶ dynamic measurement of reaction gas streams
- ▶ catalysis and thermal analysis
- ▶ molecular beam studies
- ▶ dissolved species probes
- ▶ fermentation, environmental and ecological studies

Surface Science




- ▶ UHVTPD
- ▶ SIMS
- ▶ end point detection in ion beam etch
- ▶ elemental imaging - surface mapping

Plasma Diagnostics



- ▶ plasma source characterization
- ▶ etch and deposition process reaction kinetic studies
- ▶ analysis of neutral and radical species

Vacuum Analysis



- ▶ partial pressure measurement and control of process gases
- ▶ reactive sputter process control
- ▶ vacuum diagnostics
- ▶ vacuum coating process monitoring

# Optimal generation of delay-controlled few-cycle pulses for high harmonic generation in solids

Cite as: Appl. Phys. Lett. **120**, 121105 (2022); doi: [10.1063/5.0085472](https://doi.org/10.1063/5.0085472)

Submitted: 17 January 2022 · Accepted: 12 March 2022 ·

Published Online: 24 March 2022




View Online



Export Citation



CrossMark

Yabei Su,<sup>1,2</sup> Shaobo Fang,<sup>2,3,4,a)</sup>  Shuai Wang,<sup>2,3</sup> Yueying Liang,<sup>2,3</sup> Guoqing Chang,<sup>2,3,4</sup> Xinkui He,<sup>2,3,4</sup> and Zhiyi Wei<sup>2,3,4</sup>

## AFFILIATIONS

<sup>1</sup>School of Physics and Optoelectronic Engineering, Xidian University, Xi'an 710071, People's Republic of China

<sup>2</sup>Institute of Physics, Chinese Academy of Sciences, Beijing 100049, People's Republic of China

<sup>3</sup>University of Chinese Academy of Science, Beijing 100049, People's Republic of China

<sup>4</sup>Songshan Lake Materials Laboratory, Dongguan, Guangdong 523808, China

<sup>a)</sup> Author to whom correspondence should be addressed: [shaobo.fang@iphy.ac.cn](mailto:shaobo.fang@iphy.ac.cn)

## ABSTRACT

Delay-controlled two-color, few-cycle pulses are powerful tools for ultrafast nonlinear optics. In this Letter, 35-fs, 800 nm pulses were injected into a noble-gas-filled hollow-core fiber to obtain over-octave spectra (450–1000 nm) and were divided into two parts for dispersion management by a Mach–Zehnder-type interferometer. Two few-cycle pulses with pulse widths of 9.3 and 4.5 fs were generated in the long-wavelength side and the short-wavelength side, respectively. The temporal profiles were measured as the function of the different delay between the two pulses. The shortest 3.6 fs, 0.75 mJ near-single-cycle pulses were synthesized at an optimal delay. The delay-controlled high-harmonic generation in MgO was experimentally demonstrated leading to twofold enhancement of high-order harmonic (HH) yields at 10.3 eV and the extension of HH frequency under time-delay modulation. This method provides an extensive way for manipulating delay-controlled multi-color pulses, which can be used for controlling ionization dynamics in extreme nonlinear optics. We believe that it will be a powerful tool for ultrafast science.

Published under an exclusive license by AIP Publishing. <https://doi.org/10.1063/5.0085472>

Thanks to the development of the post-compression technique, attosecond science has made tremendous progress in the past two decades.<sup>1</sup> Nowadays, isolated attosecond pulses (IAPs) can be routinely generated based on high harmonic generation in gases. Since the most intriguing strong-field pump-probe experiments require intense IAPs, the driving sources have been experimentally improved for boosting the yields of high-order harmonic (HH). For example, nano-joule IAPs were produced by utilizing near single-cycle driving pulses<sup>2</sup> and micro-joule IAPs were reported by using two-color, multi-cycle pulses gating technology.<sup>3</sup> The latest theoretical study showed that HH yields in gases were greatly enhanced by time-delay modulation between two-color, few-cycle pulses.<sup>4</sup>

During the last decade, solid-state high-harmonic generation (HHG) has been experimentally observed and became a hot topic in ultrafast science.<sup>5</sup> Although the physical mechanisms of solid-state HHG were disputably explained by interband and intraband excitations, the HH emission from solids readily shows great application prospects, e.g., petahertz electronics, compact extreme ultraviolet (EUV) sources, IAPs, and reconstruction of electronic band structures.<sup>6–9</sup>

Recently, several theoretical studies showed that the significant enhancement of the HH yields and the extension of HH cutoff photon energy in solids can be obtained by varying the relative delay<sup>10</sup> or phase<sup>11</sup> of two-color, few-cycle fields. Therefore, generation of intense two or multi-color, few-cycle optical fields is crucial for studying these ultrafast phenomena. Using parametric waveform synthesizer, two<sup>12,13</sup> or three channels<sup>14</sup> few-cycle pulses have been obtained. Single-cycle or even sub-cycle light fields can be synthesized. However, these systems are relatively complex due to the required multi-stage parametric amplifiers. An alternative is using a static gas-filled hollow-core fiber (HCF) to produce the white-light supercontinuum, which is then split into multiple channels with the dispersion in each channel being compensated by chirped mirrors. This technique also makes it possible to obtain multi-channel few-cycle pulses, even synthesized sub-cycle pulses.<sup>15,16</sup> However, the ionization effects in the front end of a static gas-filled HCF limit the energy of the white-light supercontinuum less than 1 mJ.

Here, we experimentally generated two-color, few-cycle pulses, which can be optimized and shaped to millijoule-level 1.5 cycle pulses

using two channels to manage dispersion based on a pressure gradient neon-gas-filled HCF. This method provides an option of time-delay modulation of the pulse profiles. When the pulses have only a few oscillations, a time delay between two pulses and the carrier-envelope phase (CEP) both have a great impact on the overall pulse envelope. The HH yields are equivalently sensitive to the CEP<sup>17</sup> and time delays<sup>10</sup> in multi-color, few-cycle laser fields. Using the two-color, few-cycle pulses, the quantitative studies of the time-delay-dependent HH radiation in solids were further experimentally performed.

The experimental post-compression setup is shown in Fig. 1. The front-end source was a Ti:sapphire regenerative amplifier with the pulse width of 35 fs and beam diameter of 13 mm ( $1/e^2$  of the intensity profile) at 1 kHz. The laser beam was loosely focused into the HCF with a 400- $\mu\text{m}$  inner diameter and 0.9-m length using an  $f=2.5$  m concave focusing mirror. To reduce ionization, the front end and back end of the fiber were separated to create the effect of pressure gradient. The  $1/e^2$  radius of the input beam waist of Gaussian shape was 260  $\mu\text{m}$  to ensure maximum energy coupled into the  $\text{EH}_{11}$  mode of the HCF. The coupling efficiency is over 98% according to the theoretical calculations.<sup>18</sup> The HCF was placed on a metal groove to keep straight, and the whole devices were enclosed in a stainless-steel tube filled with noble gas. The front and back of the stainless-steel tube was sealed by optical window made of fused quartz. The anti-reflection coated windows from 450 to 1000 nm were glued on stainless steel tube at Brewster's angle to ensure linear p-polarization. The thicknesses of the windows were 0.5 mm of the front window and 1 mm of the end window respectively. The divergent beam exiting the HCF was re-collimated by a spherical silver-coated mirror ( $f=2$  m). The supercontinuum was guided into a Mach-Zehnder-type interferometer including a beam splitter and a beam combiner. The spectrum through the beam splitter was the long-wavelength part from 700 to 1000 nm,

and the reflection spectrum was the short-wavelength part from 450 to 700 nm, this is because that the pulses at the short side were more susceptible to suffer from distortion by dispersion. Two set of custom-designed chirped mirrors were used to compensate for dispersion, and the dispersion in each channel was finely tuned with a pair of wedges. For the establishment of Mach-Zehnder interferometer and the adjustment of the time delay, the short-wavelength channel contained a delay stage. After the beam combiner, a flip mirror guided the synthesized pulses to a D-scan (d-scan B, Sphere Ultrafast Photonics Inc.) setup, which has the advantages of retrieving the full pulse information rapidly and giving optimized solution for dispersion compensation as shown in previous work.<sup>19</sup> The distance from the flip mirror to the D-scan was equal to the distance from the flip mirror to the vacuum cavity of HHG. When measuring pulse width, a 0.5 mm thick window coating anti-reflection films from 450 to 1000 nm, which was the same as the window of the HHG-cavity, was placed before the D-scan. This was to ensure that the measured pulses were the same as those used in the HHG experiments.

The HHG setup was inside a vacuum chamber, which is shown in Fig. 2. An aperture was placed before the vacuum chamber window to control the laser intensity for optimized HH results. We used a spherical mirror ( $f=1300$  mm) to directly focus the two-color, few-cycle pulses to a 001-cut 200  $\mu\text{m}$ -thick MgO crystal, which was mounted on a translation platform. The HH spectra were characterized by a flat-field XUV spectrometer. The slit was imaged by a concave gold grating with 600 grooves/mm in the vertical (spectral) dimension on a dual micro-channel plate (MCP) detector equipped with a phosphor screen and observed with a CCD camera.

The 35-fs input pulses with 1.7-mJ pulse energy were focused into the hollow-core capillary, and the output was 1.25 mJ corresponding to a transmittance of 75%, which was close to loss of theoretical

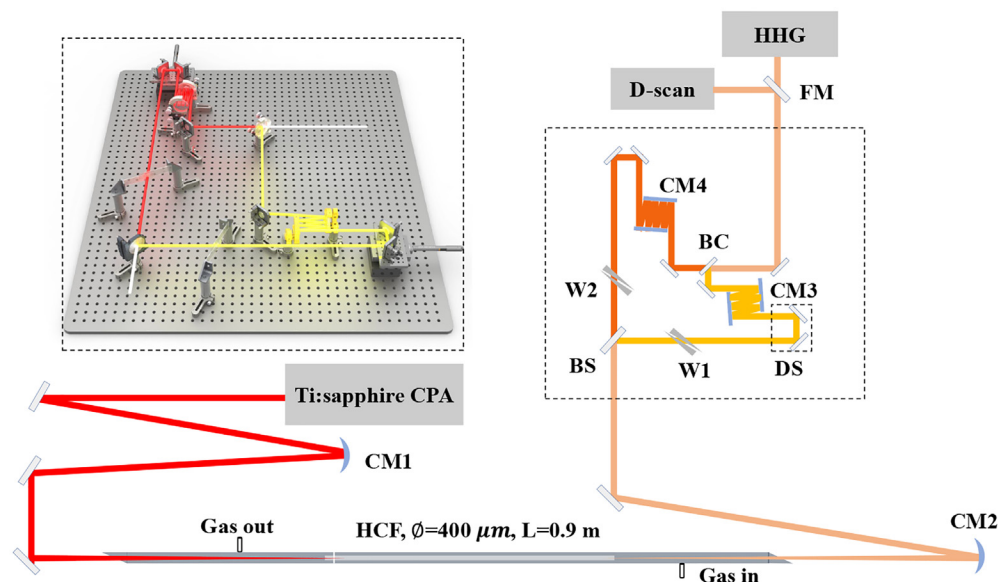


**FIG. 1.** Schematic of experimental setup. CM1-2, curved mirror; W1-2, wedges; CM3-4, chirped mirrors; BS, beam splitter; BC, beam combiner; DS, delay stage; and FM, flip mirror; the inset at the top left corner shows three-dimensional image of the interferometer.

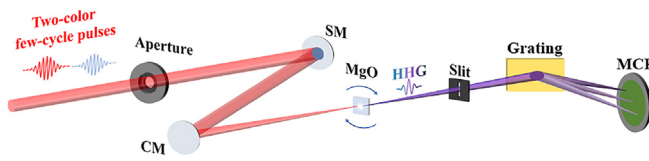


**FIG. 2.** Experimental setup for HHG. SM, silver mirror; CM, curved mirror; and MCP, micro-channel plate.

calculations.<sup>20</sup> This means that the system minimizes ionization loss and bending loss of the capillary. After the beam splitter, the energy of the long side was 0.91 mJ and the energy of the short side was 0.21 mJ. After the interferometer, the total energy was 0.75 mJ. The energy of the long-wavelength side was 0.67 mJ corresponding to an efficiency of 74%. The energy of the short-wavelength side was 0.08 mJ corresponding to an efficiency of 38%. The loss of the Mach-Zehnder-type interferometer was mainly due to the transmission loss of chirped

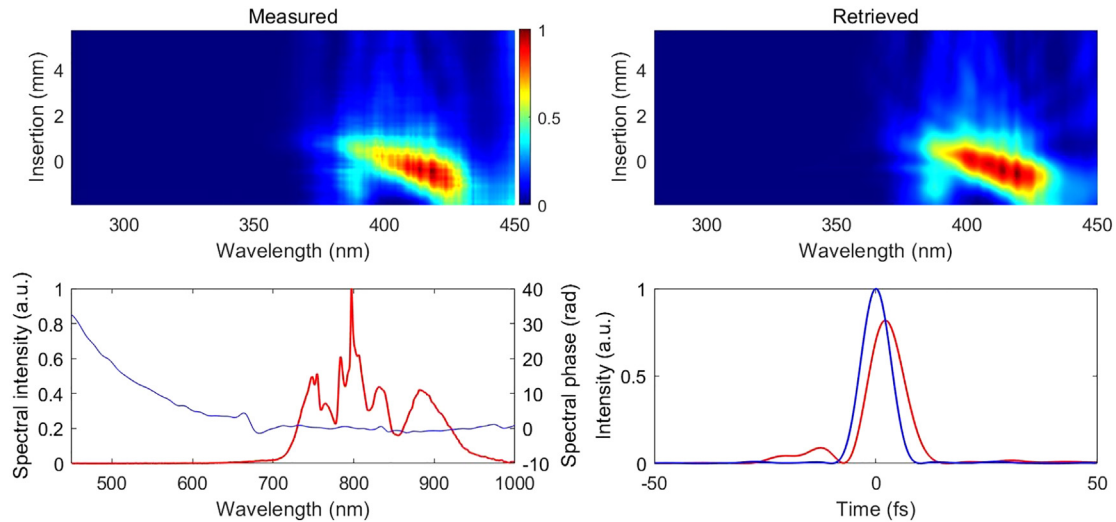


**FIG. 3.** Measured (a) and retrieved (b) SHG d-scan trace of the long-wavelength side. (c) Measured experimental spectrum (red line) and retrieved spectral phase (blue line). (d) The retrieved temporal pulse shape of 9.3 fs (red line) and the transform-limited shape of 8.3 fs (blue line).

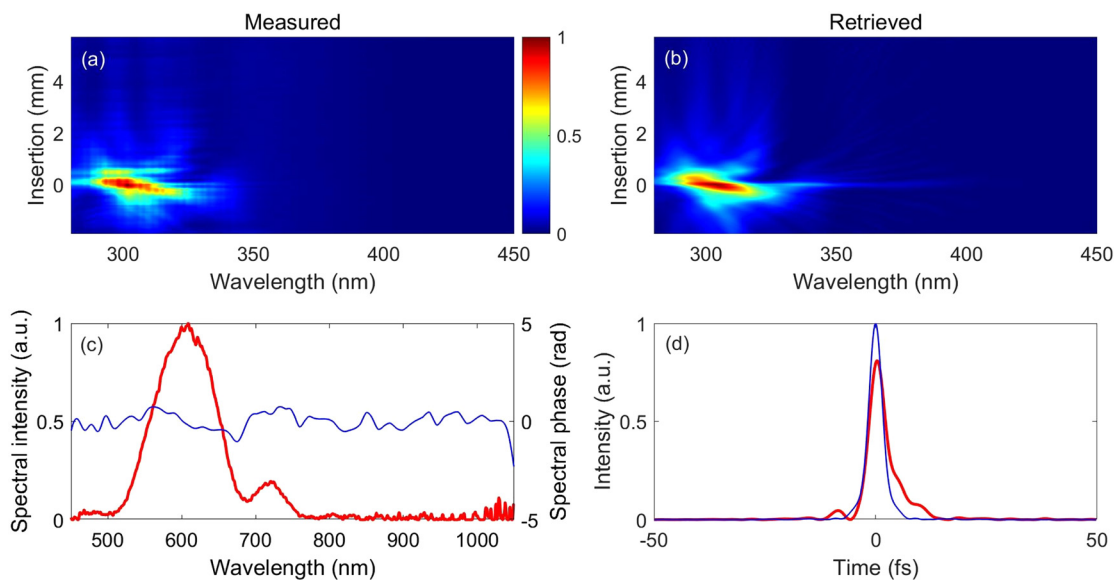


**FIG. 4.** Measured (a) and retrieved (b) SHG d-scan trace of the short-wavelength side. (c) Measured experimental spectrum (red line) and retrieved spectral phase (blue line). (d) The retrieved temporal pulse shape of 4.5 fs (red line) and the transform-limited shape of 3.6 fs (blue line).



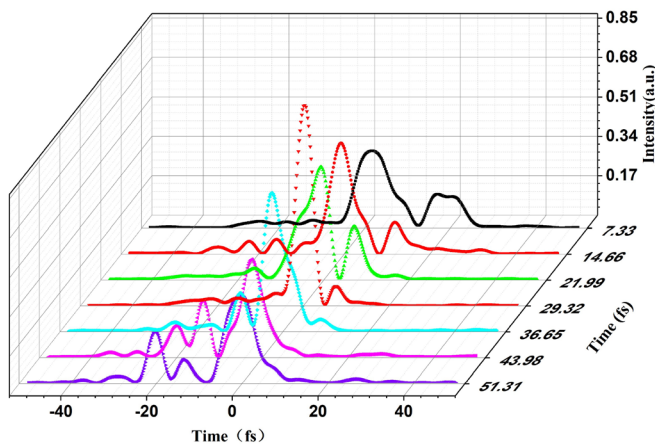


**FIG. 5.** Measured the evolution of the intensity profile of the two-color few-cycle pulses. The short-wavelength side pulse moved from the back edge of the long-wavelength side pulse to the front via step by step of 7.33 fs.

mirrors, the reflection loss of wedge pairs and apertures in the optical path. In our experiment, we found that the neon of 2.6 bar in absolute pressure filled at the end of the HCF was the most optimal for obtain high-quality pulse compression. Above than 2.6 bar, broader spectrum could be obtained with a strong characteristic of blue shift due to the increased ionization. However, higher-order dispersion due to the ionization made it difficult to achieve high-quality pulse compression using the custom-designed chirped mirrors. At the same time, the beam quality deteriorated, the intensity of the spectrum became unstable and the transmission of the HCF was reduced rapidly. At 2.6 bar, the stable spectrum spanned from 450 to 1000 nm, supporting transform-limited pulse duration of 3.2 fs. Figures 3–6 show the

measured pulse widths of the post compression after the neon-filled HCF. The spectrum spanning from 700 to 1000 nm of the long-wavelength side supported transform-limited pulse of 8.3 fs. The temporal profile of the long-wavelength side pulse is represented in Fig. 3(d) (red curve), and the pulse duration was 9.3 fs (1.4% reconstruction error) corresponding to 3.4 optical cycles at the center wavelength of 816 nm. The spectrum spanning from 450 to 700 nm of the short-wavelength side supported transform-limited pulse of 3.6 fs. The temporal profile of the short-wavelength side pulse is represented in Fig. 4(d) (red curve), and the pulse duration was 4.5 fs (1.6% reconstruction error) corresponding to 2.2 optical cycles at the center wavelength of 627 nm. The controllability of the intensity profiles by time delays of the two pulses is shown in Fig. 5. The time interval for each adjustment was 7.33 fs. Optimizing the time delays between the two channels, the temporal profile of the shortest synthesized pulse is represented in Fig. 6(d). The shortest pulse width (red curve) was 3.6 fs (2.5% reconstruction error) corresponding to 1.5 optical cycles at the center wavelength of 712 nm and close to the transform-limited pulse of 3.2 fs.

To demonstrate the effect of time-delay modulation of the two-color few-cycle pulses in ultrafast nonlinear optics, we investigated the solid-state HHG in MgO (bandgap of 7.8 eV), which has been proved an excellent crystal for HHG.<sup>21</sup> The evolution of the HH spectra via different delays between the two arms is shown in Fig. 7(a). The pulses with total energy of 300  $\mu$ J (220  $\mu$ J) of long-wavelength side and 80  $\mu$ J of short-wavelength side) were focused into the crystal, and higher energy was more likely to destroy the crystal. We estimated the peak intensities inside the crystal to be 16 and 10 TW/cm<sup>2</sup> for the long and short-wavelength side pulses, respectively. The HH spectra generated using one of the channels are shown in Fig. 7(b). The HH spectra mainly presented two characteristics by the time-delay modulation. First, when the time interval between the peaks of two pulses was within 6 fs measured by the extra-cavity D-scan, the spectra at 13.4–14.6 eV was expanded.

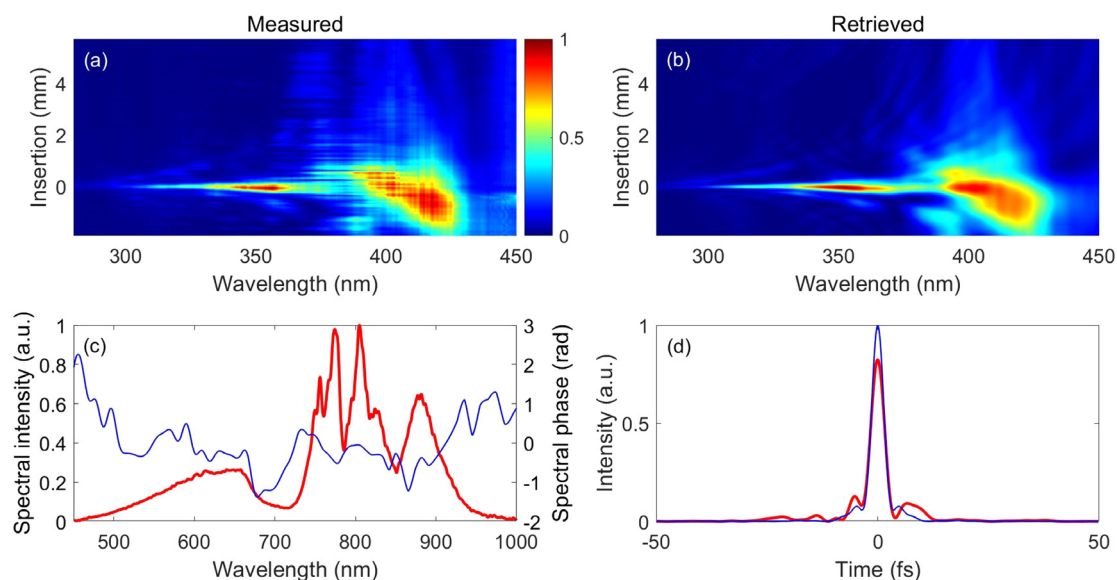


**FIG. 6.** Measured (a) and retrieved (b) SHG d-scan trace of the optimal synthesized pulse. (c) Measured experimental spectrum (red line) and retrieved spectral phase (blue line). (d) The retrieved temporal pulse shape of 3.6 fs (red line) and the transform-limited shape of 3.2 fs (blue line).

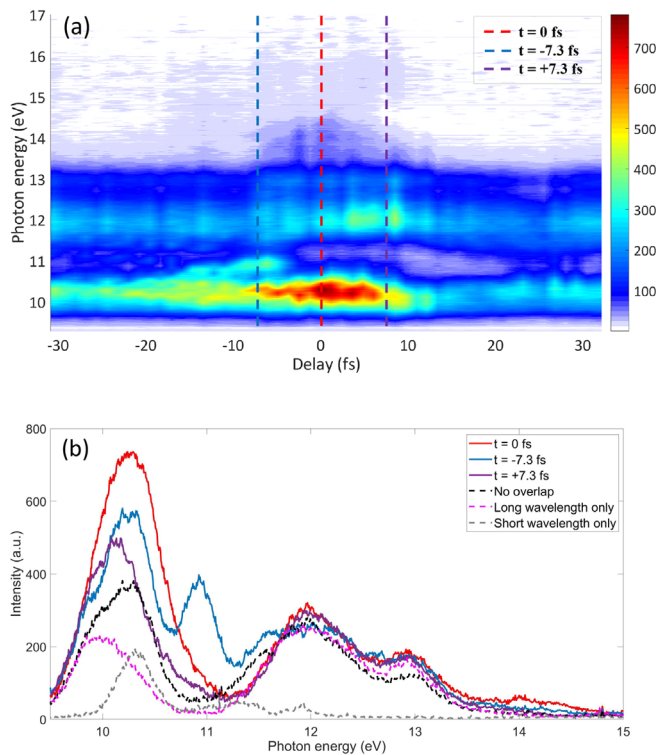


**FIG. 7.** (a) Measured the evolution of the XUV spectra via step by step of 1.22 fs. (b) XUV spectra at  $t = 0$  fs (red solid curve),  $t = -7.3$  fs (blue solid curve),  $t = +7.3$  fs (purple solid curve), full separation in time of the two pulses (black dashed curve), long wavelength only (pink dashed curve), and short wavelength only (gray dashed curve).

We assumed that the maximal cutoff photon energy appeared at the zero point ( $t = 0$ ) and there was twofold enhancement of the HH yields at 10.3 eV compared to that the two pulses were fully separated in time and had no mutual influence, which is shown in Fig. 7(b). Second, the HH spectra were asymmetric about both sides of the zero point. When the pulses of the short-wavelength side first interacted with the crystal ( $t < 0$ ), the spectral intensity was enhanced especially at 11 eV compared to that the pulses of the long-wavelength side first interacted with the crystal ( $t > 0$ ). For example, in Fig. 7(b), the spectra at 11 eV were shown at  $t = \pm 7.3$  fs. The physical process can be depicted by the three-step model in momentum space for solids.<sup>22</sup> When the electron-hole pairs (interband transition) were first induced by the short-wavelength side pulses, and the following long-wavelength side pulses controlled the intraband motion and electron-hole collisions,<sup>23</sup> this led to enhanced yields at specific frequency. When two pulses drove the process almost simultaneously, the enhancement was observed at around 10.3 eV and the cutoff photon energy extended. With decreasing time intervals of the two-channel pulses, they interfered into a shorter pulse and the peak power increased. Since the cutoff photon energy scales linearly with driven laser field,<sup>5</sup> the cutoff photon energy increases when the intensity of the synthesized laser field increases. We have experimentally demonstrated that it is possible to use the delay-controlled two-color fields to control the electron motions in the solids and achieve favorable HH emission.

In conclusion, we report a compact Mach-Zehnder-type interferometer for dispersion management of an over-octave spanning spectrum. Using this setup, we obtained intense two-color few-cycle laser pulses, which can be synthesized to 0.75-mJ 3.6-fs pulses, corresponding to 1.5 optical cycles at the center wavelength of 712 nm. The effect of time-delay modulation of the two-color few-cycle pulses was demonstrated. Furthermore, we experimentally demonstrated that the delay-controlled, two-color, few-cycle pulses can be used as a sensitive means to control and enhance the solid-state HH emission in MgO. This approach shows the great potential for the development of attosecond sources by efficiency solid-state HHG. We foresee that the stable enhanced HH spectra will help to understand the mechanism of HHG in solids and the delay-controlled few-cycle laser source will be a versatile tool for manipulating trajectories of an electron in HHG, IAP-generation, strong-field physics, and ultrafast spectroscopy.

S. Fang gratefully acknowledges support from Professor Mikio Yamashita and Professor Franz X. Kärtner. This work was supported by National Key R&D Program of China (Nos. 2020YFB1313702 and 2017YFC0110301), National Natural Science Foundation of China (No. 91950113 and 61575219), Scientific Instrument Developing Project of Chinese Academy of Sciences (Nos. YJKYYQ20210025 and YJKYYQ20180046), Chinese Academy of Sciences Key Technology Talent Program (2019), Youth Innovation Promotion Association CAS (No. 2018007) and the Synergetic Extreme Condition User Facility (SECUF).

## AUTHOR DECLARATIONS

### Conflict of Interest

The authors have no conflicts to disclose.

## DATA AVAILABILITY

The data that support the findings of this study are available from the corresponding author upon reasonable request.

## REFERENCES

- <sup>1</sup>F. Krausz and M. Ivanov, *Rev. Mod. Phys.* **81**, 163 (2009).
- <sup>2</sup>H. Timmers, Y. Kobayashi, K. F. Chang, M. Reduzzi, D. M. Neumark, and S. R. Leone, *Opt. Lett.* **42**, 811 (2017).
- <sup>3</sup>E. J. Takahashi, P. Lan, O. D. Mücke, Y. Nabekawa, and K. Midorikawa, *Nat. Commun.* **4**, 2691 (2013).
- <sup>4</sup>D. Peng, L.-W. Pi, M. V. Frolov, and A. F. Starace, *Phys. Rev. A* **95**, 033413 (2017).
- <sup>5</sup>S. Ghimire, A. D. DiChiara, E. Sistrunk, P. Agostini, L. F. DiMauro, and D. A. Reis, *Nat. Phys.* **7**, 138 (2011).
- <sup>6</sup>M. Garg, M. Zhan, T. T. Luu, H. Lakhota, T. Klostermann, A. Guggenmos, and E. Goulielmakis, *Nat.* **538**, 359 (2016).
- <sup>7</sup>T. T. Luu, V. Scagnoli, S. Saha, L. J. Heyderman, and H. J. Wörner, *Opt. Lett.* **43**, 1790 (2018).
- <sup>8</sup>Z. Nourbakhsh, N. Tancogne-Dejean, H. Merdji, and A. Rubio, *Phys. Rev. Applied* **15**, 014013 (2021).
- <sup>9</sup>A. A. Lanin, E. A. Stepanov, A. B. Fedotov, and A. M. Zheltikov, *Optica* **4**, 516 (2017).
- <sup>10</sup>F. Navarrete and U. Thumm, *Phys. Rev. A* **102**, 063123 (2020).
- <sup>11</sup>M. Guan, S. Hu, H. Zhao, C. Lian, and S. Meng, *Appl. Phys. Lett.* **116**, 043101 (2020).
- <sup>12</sup>S.-W. Huang, G. Cirmi, J. Moses, K.-H. Hong, S. Bhardwaj, J. R. Birge, L.-J. Chen, E. Li, B. J. Eggleton, G. Cerullo, and F. X. Kärtner, *Nat. Photonics* **5**, 475 (2011).
- <sup>13</sup>Y. C. Lin, Y. Nabekawa, and K. Midorikawa, *Nat. Commun.* **11**, 3413 (2020).

- <sup>14</sup>O. D. Mücke, S. B. Fang, G. Cirimi, G. M. Rossi, S.-H. Chia, H. Ye, Y. Yang, R. Mainz, C. Manzoni, P. Farinello, G. Cerullo, and F. X. Kärtner, *IEEE J. Sel. Top. Quantum Electron.* **21**, 8700712 (2015).
- <sup>15</sup>A. Wirth, M. T. Hassan, I. Grguras, J. Gagnon, A. Moulet, T. T. Luu, S. Pabst, R. Santra, Z. A. Alahmed, A. M. Azzeer, V. S. Yakovlev, V. Pervak, F. Krausz, and E. Goulielmakis, *Science* **334**, 195 (2011).
- <sup>16</sup>M. T. Hassan, T. T. Luu, A. Moulet, O. Raskazovskaya, P. Zhokhov, M. Garg, N. Karpowicz, A. M. Zheltikov, V. Pervak, F. Krausz, and E. Goulielmakis, *Nature* **530**, 66 (2016).
- <sup>17</sup>T. T. Luu, M. Garg, S. Y. Kruchinin, A. Moulet, M. T. Hassan, and E. Goulielmakis, *Nature* **521**, 498 (2015).
- <sup>18</sup>M. Nisoli, S. Stagira, S. De Silvestri, O. Svelto, S. Sartania, Z. Cheng, G. Tempea, C. Spielmann, and F. Krausz, *IEEE J. Select. Top. Quantum Electron.* **4**, 414 (1998).
- <sup>19</sup>M. Miranda, T. Fordell, C. Arnold, A. L'Huillier, and H. Crespo, *Opt. Express* **20**, 688 (2012).
- <sup>20</sup>E. A. J. Marcatili and R. A. Schmeltzer, *Bell. Syst. Tech. J.* **43**, 1783 (1964).
- <sup>21</sup>Y. S. You, D. A. Reis, and S. Ghimire, *Nat. Phys.* **13**, 345 (2017).
- <sup>22</sup>G. Vampa, C. R. McDonals, G. Orlando, D. D. Klug, P. B. Korkum, and T. Brabec, *Phys. Rev. Lett.* **113**, 073901 (2014).
- <sup>23</sup>F. Langer, M. Hohenleutner, C. P. Schmid, C. Pöhlmann, P. Nagler, T. Korn, C. Schüller, M. S. Sherwin, U. Huttner, J. T. Steiner, S. W. Koch, M. Kira, and R. Huber, *Nature* **533**, 225 (2016).